

Thermal superconducting quantum interference proximity transistor

Nadia Ligato,^{1,2} Federico Paolucci,^{1,2} Elia Strambini,¹ and Francesco Giazotto^{1,*}

¹*NEST, Istituto Nanoscienze-CNR and Scuola Normale Superiore, I-56127 Pisa, Italy*

²*These authors equally contributed to the work.*

Superconductors are known to be excellent thermal insulators at low temperature owing to the presence of the energy gap in their density of states (DOS) [1]. In this context, the superconducting *proximity effect* [2] allows to tune the local DOS of a metallic wire by controlling the phase bias (φ) imposed across it [3]. As a result, the wire thermal conductance can be tuned over several orders of magnitude by phase manipulation [1]. Despite strong implications in nanoscale heat management, experimental proofs of phase-driven control of thermal transport in superconducting proximitized nanostructures are still very limited [4–6]. Here, we report the experimental demonstration of efficient heat current control by phase tuning the superconducting proximity effect. This is achieved by exploiting the magnetic flux-driven manipulation of the DOS of a quasi one-dimensional aluminum nanowire forming a weak-link embedded in a superconducting ring [7, 8]. Our thermal superconducting quantum interference transistor (T-SQUIPT) shows temperature modulations up to ~ 16 mK yielding a temperature-to-flux transfer function as large as ~ 60 mK/ Φ_0 . Yet, phase-slip transitions occurring in the nanowire Josephson junction induce a hysteretic dependence of its local DOS on the direction of the applied magnetic field. Thus, we also prove the operation of the T-SQUIPT as a phase-tunable *thermal memory* [9, 10], where the information is encoded in the temperature of the metallic mesoscopic island. Besides their relevance in quantum physics, our results are pivotal for the design of innovative coherent caloritronics devices [11, 12] such as heat valves [13] and temperature amplifiers [14] suitable for thermal logic architectures [15].

Thermal transport in superconductors stems from quasiparticle excitations only, since Cooper pairs are unable to carry heat [1]. At low temperature, the presence of quasiparticles is exponentially damped [16] thanks to the amplitude of the energy gap ($E_g \gg k_B T$, where k_B is the Boltzmann constant and T the temperature) present in the DOS so that superconductors turn out to be excellent thermal insulators [1]. Similarly, the heat current (P_{NIS}) flowing from a normal metal (N , at temperature T_N) to a tunnel-coupled superconductor (S , at temperature T_S) in a temperature-biased NIS junction (where

I indicates an insulating tunnel barrier and $T_N > T_S$) is heavily suppressed when the thermal energy is much lower than E_g [1]. For a given temperature gradient, P_{NIS} can rise by several orders of magnitude by lowering E_g , as shown in Fig. 1a (see Methods for details). Yet, in a proximitized superconductor (S') the superconducting energy gap ($E_{g'}$) can be finely controlled by tuning the macroscopic quantum phase across it (φ) [2, 3] so that thermal transport through a NIS' tunnel junction is, in principle, φ -tunable [11, 12]. The integration of S' in a superconducting loop (see Fig. 1b) allows to control φ [7, 8] and thereby to modulate its thermal properties [1, 13] with an external magnetic flux piercing the ring area (Φ). The possibility to Φ -tune the thermal conductance of a proximitized normal metal was demonstrated in Andreev interferometers showing a limited temperature modulation ($\delta T < 0.5$ mK) [4–6]. A larger control of the heat transport properties in proximitized systems would enable the development of the thermal counterparts of widespread electronic devices [11, 12], such as transistors [14], logic gates [15], and memories [9, 10].

Here, by exploiting a temperature-biased NIS' junction embedded in a superconducting ring [7, 8] we realize a thermal superconducting quantum interference proximity transistor (T-SQUIPT) [13] based on the phase-driven manipulation of the heat current ($P_{NIS'}$) via proximity effect. The implementation of our T-SQUIPT is shown in the false-color scanning electron micrograph presented in Fig. 1c. The device was realized by standard nano-fabrication techniques employing conventional metals (see Methods for fabrication details). The S' element consists of a 380-nm-long quasi one-dimensional aluminum wire (yellow, $w = 90$ nm and $t = 20$ nm), while the superconducting ring (S_R) is made of a 70-nm-thick Al layer (blue). The N reservoir (red, 15-nm-thick $\text{Al}_{0.98}\text{Mn}_{0.02}$) is coupled to S' via an AlMn-Ox tunnel junction with normal-state resistance $R_T \simeq 65$ k Ω . To perform thermal transport experiments, a series of superconducting aluminum heaters/thermometers (yellow, 25-nm-thick) [1] are tunnel coupled to N (see Methods for details).

The charge transport properties of the T-SQUIPT is reported elsewhere [17]. In particular, the electronic tunneling current is modulated by the external magnetic flux with the expected Φ_0 -periodicity (where $\Phi_0 \simeq 2.067 \times 10^{-15}$ Wb is the flux-quantum), together with a hysteresis associated to the phase-slip transition typical of *long* $S_R S' S_R$ junctions [3, 8, 18]. We exploit the same structure to prove the phase-coherent control of heat current $P_{NIS'}(\Phi)$. Thermal measurements are performed by recording the electronic temperature in N [$T_N(\Phi)$]

* francesco.giazotto@sns.it

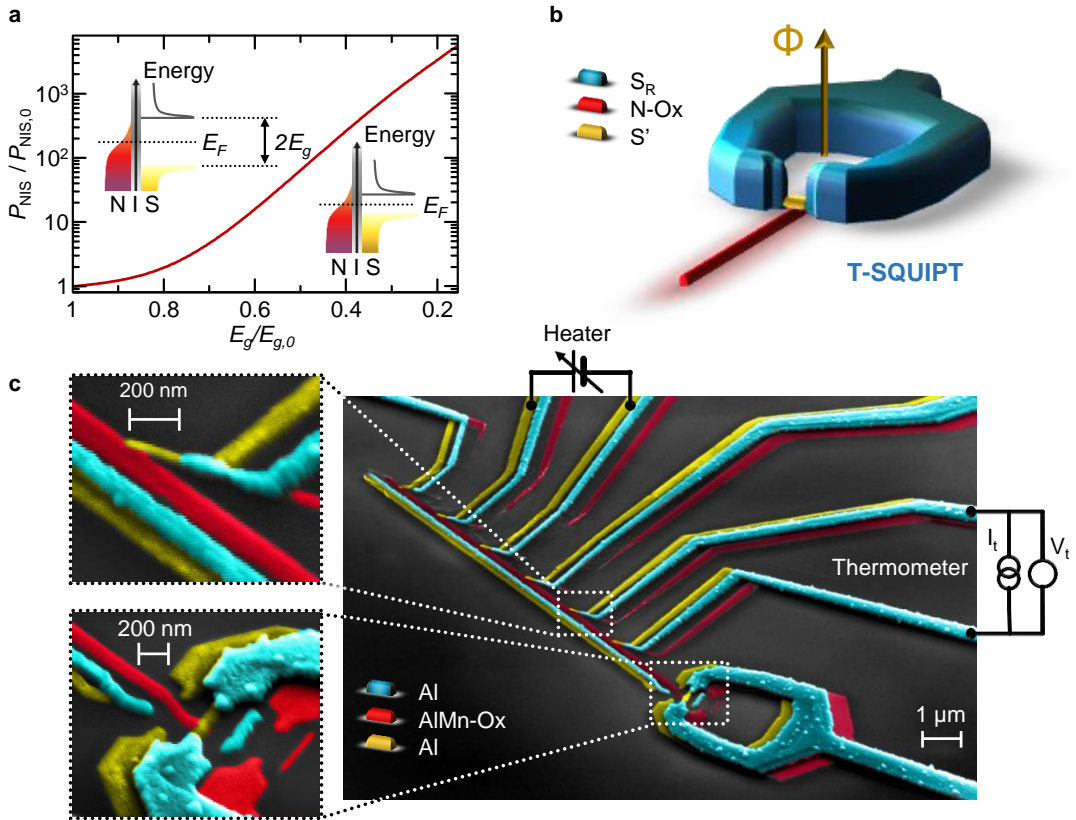


FIG. 1. Thermal superconducting quantum interference proximity transistor operation principle and implementation. **a** Normalized thermal current through a NIS tunnel junction (i.e., $P_{NIS}/P_{NIS,0}$) versus normalized energy gap of S (i.e., $E_g/E_{g,0}$). $E_{g,0}$ is the maximum value of the energy gap, while $P_{NIS,0}$ is the thermal current for $E_{g,0}$ at constant temperature gradient across the junction. Here, we set $T_N = 0.1T_{C,0}$ and $T_S = 0.01T_{C,0}$, where $T_{C,0}$ is the superconducting critical temperature corresponding to $E_{g,0}$. A decrease of E_g of about 85% causes an enhancement of P_{NIS} of almost 4 orders of magnitude. Insets: Schemes of the energy band diagram of a temperature biased NIS junction. E_F denotes the Fermi energy. **b** Sketch of the thermal superconducting quantum interference proximity transistor (T-SQUIPT). A proximitized superconducting nanowire (S' , yellow) is phase-biased via a magnetic flux (Φ) piercing a superconducting loop (S_R , blue). A normal metal electrode (N , red) is tunnel-coupled to S' to form a NIS' junction. The T-SQUIPT is operated by setting different electronic temperatures in S' and N . **c** False-color scanning electron micrograph of a typical T-SQUIPT. An Al nanowire (S' , yellow) is inserted in an Al ring (S_R , blue), while an $Al_{0.98}Mn_{0.02}$ normal metal electrode (N , red) is tunnel-coupled to the middle of the nanowire. A set of superconducting aluminum tunnel probes (yellow) are coupled to N , and serve as local heaters and thermometers. Insets: blow-up of a thermometer (top) and the NIS' region (bottom).

while heated by a constant power P_{in} at fixed bath temperature (T_b), as depicted in Fig. 2a (see Methods for details). The resulting temperature gradient set across the NIS' junction gives rise to a finite thermal current $P_{NIS'}(\Phi)$, which is the only Φ -dependent heat exchange channel for N (see Methods for details). As a consequence, the variation of T_N with the magnetic flux arises only from the modulation of $E_{g'}(\Phi)$ via the proximity effect, as sketched in Fig. 2b.

Figure 2c shows T_N as a function of Φ measured for $P_{in} = 3.2$ pW at 25 mK. Stemming from Φ -modulation of $P_{NIS'}$, T_N is Φ_0 -periodic and is hysteretic with the sweep direction of Φ , similarly to the electronic counterpart [17]. The strong suppression of $P_{NIS'}$ occurring for $\Phi = 0$ [where $E_{g'}(0)$ is maximal] yields the maximum steady-state electronic temperature established in

N (T_{MAX}), while thermal current enhancement at higher magnetic fluxes causes the decrease of T_N down to its minimum (T_{min}). Notably, T_{min} is not recorded exactly at $\Phi = 0.5\Phi_0$ and hysteretic in the magnetic flux as a consequence of the phase-slip transitions occurring in S' [3, 8, 17, 18].

Let us now investigate the impact of P_{in} on the performance of the T-SQUIPT. Figure 2d shows the $T_N(\Phi)$ characteristics measured at 25 mK for three selected values of P_{in} . At a given Φ , the value of T_N monotonically rises by increasing the input power, as shown in the inset of Fig. 2e. Similarly, the temperature modulation (δT) grows with the input power. In particular, the T-SQUIPT shows a maximum $\delta T \sim 16$ mK for $P_{in} = 12$ pW, which corresponds to a relative variation of T_N of about 1.7%.

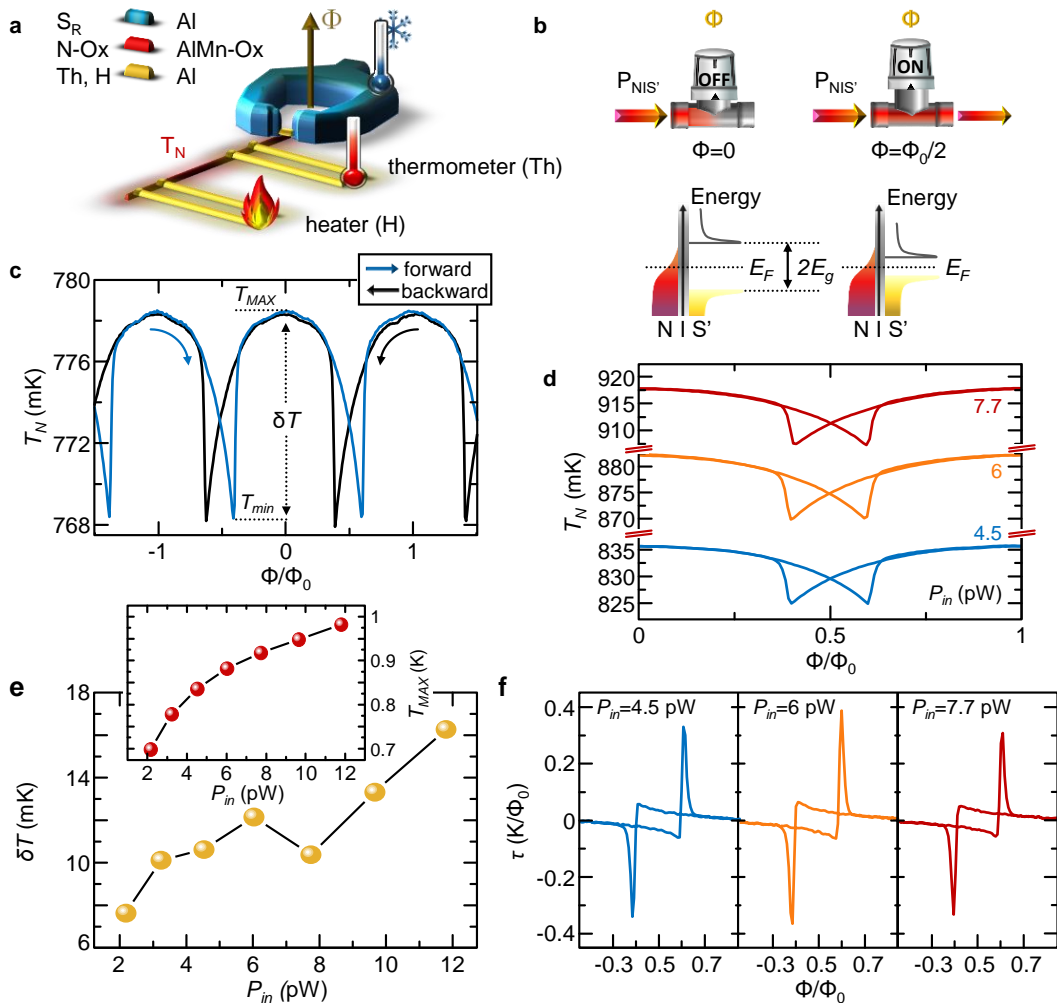


FIG. 2. Low temperature behavior of the T-SQUIPT. **a** Sketch of the thermal setup of the T-SQUIPT. The electronic temperature (T_N) in the N electrode (red, $\text{Al}_{0.98}\text{Mn}_{0.02}$) is raised by injecting power through a pair of superconducting heaters, and is measured via a pair of superconducting thermometers. All these S electrodes (yellow, Al) are tunnel-coupled to N. **b** Schematic representation of the magnetic flux control of the heat current ($P_{NIS'}$) flowing through the T-SQUIPT. The flux tunes the energy gap of S' ($E_{g'}$): In particular, $E_{g'}(\Phi)$ is maximum for $\Phi = 0$ [$P_{NIS'}(0)$ is minimum] and is strongly suppressed for $\Phi = \Phi_0/2$ ($P_{NIS'}$ is enhanced). **c** Electronic temperature [$T_N(\Phi)$] of N acquired at 25 mK for $P_{in} = 3.2$ pW. The blue (forward) and black (backward) traces show different magnetic flux sweep directions. The maximum (T_{MAX}) and minimum (T_{min}) values of T_N together with the temperature swing (δT) are indicated. **d** Electronic temperature [$T_N(\Phi)$] of N acquired at 25 mK for different values of P_{in} . **e** Dependence of the electronic temperature swing (δT) on the injected power (P_{in}). δT raises with P_{in} within the explored range of heating power. Inset: Maximum electronic temperature (T_{MAX}) versus P_{in} . T_{MAX} monotonically increases with P_{in} . **f** Electronic temperature-to-flux transfer coefficient (τ) vs Φ for the same values of P_{in} shown in panel d.

The flux-to-temperature transfer coefficient ($\tau = \partial T_N / \partial \Phi$) is one key parameter to evaluate the response of the T-SQUIPT. Figure 2f shows $\tau(\Phi)$ for different values of P_{in} . Due to the highly non-linear dependence of $P_{NIS'}$ on the superconducting energy gap (see Fig. 1a), τ is vanishing for low phase-biases, and it increases up to about $60 \text{ mK}/\Phi_0$ for flux values approaching $0.5\Phi_0$. This value is on par with the first realization of a Josephson heat interferometer [19]. Furthermore, the transfer coefficient shows also a peak corresponding to the abrupt temperature change occurring at the phase-slip transi-

tion. This feature of τ cannot find practical applications, since it depends on experimental technicalities, such as the spacing and the speed of the magnetic flux sweep.

We now discuss the impact of bath temperature on the performance of the T-SQUIPT. Figure 3a displays the $T_N(\Phi)$ characteristics of the heat nanovalve measured for $P_{in} = 6$ pW at different values of T_b . At a given input power, T_{MAX} starts to rise for $T_b \geq 400$ mK, as shown in 3b. Moreover, the temperature difference between the forward and backward traces is reduced by increasing T_b , since the electron-phonon interaction in

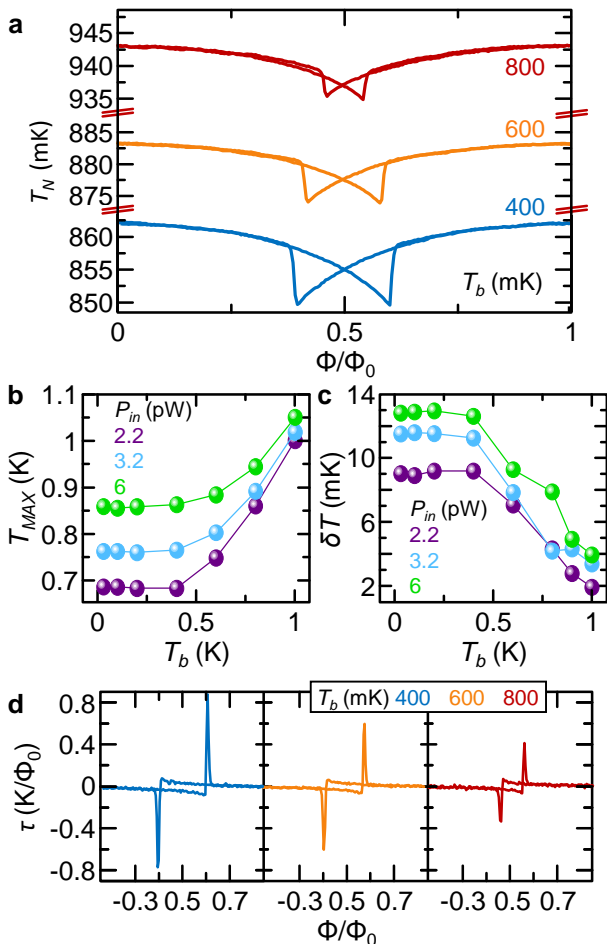


FIG. 3. **Bath temperature evolution of the T-SQUIPT behavior.** **a** Electronic temperature modulation $[T_N(\Phi)]$ of the T-SQUIPT acquired at $P_{in} = 6$ pW for different values of T_b . **b** Maximum electronic temperature in N (T_{MAX}) versus T_b for selected values of input power. For each P_{in} , T_{MAX} monotonically rises with T_b . **c** Bath temperature dependence of δT for selected values of P_{in} . The swing of T_N is rather suppressed for $T_b \gtrsim 400$ mK. **d** Flux-to-temperature transfer coefficient versus Φ at $P_{in} = 6$ pW for the same values of T_b as in panel **a**.

N becomes larger at higher bath temperatures [1, 21]. At the same time, Φ -tuning of $P_{NIS'}$ is less effective at high T_b , because the energy gap of S' is lowered while approaching its critical temperature [2] (see Methods for details). Therefore, by rising T_b the temperature swing δT for given P_{in} is damped to $\sim 20\%$ of its low temperature value (see Fig. 3c). Notably, the transfer coefficient τ is only slightly affected by the decrease of δT . As a matter of fact, $\tau(\Phi = 0.5\Phi_0)$ remains almost constant by increasing the bath temperature, as shown in Fig. 3d. By contrast, the hysteresis in the T_N versus Φ traces is reduced by raising T_b , since the S' coherence length $[\xi_{S'}(T) \propto E_g(T)^{-1/2}]$ becomes larger at higher temperatures [16] (see Methods for details) thereby causing the nanowire transition towards the short-junction

limit [3, 8].

Our T-SQUIPT may find application as a phase-tunable memory element suitable for *thermal computing* [15]. Indeed, in full analogy with superconducting electronic memories [17, 22–24], the hysteretic $T_N(\Phi)$ characteristics can be exploited to store logic information, as schematically shown in Fig. 4a. In the T-SQUIPT, the two distinct temperature states (i.e., *low* [0] and *high* [1]) at the read out flux (Φ_R) are characterized by a different *topological* index, and can be discriminated by the parity of the winding number of φ along the Al wire (*odd* or *even*) [17, 18]. These states are only accessible by sweeping the magnetic flux in opposite directions, as demonstrated in the electrical counterpart [17]. Indeed, writing (erasing) the T-SQUIPT is performed by temporarily rising (lowering) the total flux above (below) the hysteresis loop. Unwanted stochastic transitions (due, for instance, to quantum tunneling or thermal activation) are prevented in the T-SQUIPT by the large phase-slip energy barrier [18] present in the wire thereby making the phase-slip rate vanishing up to about the superconducting critical temperature [17]. This enables the use of the T-SQUIPT as a *persistent thermal memory cell*.

The primary thermal memory cell operation is based on a continuous read-mode, which requires a permanent power injection P_{in} in the N region. In Fig. 4b, the device is powered with 4.5 pW and the read-out flux is set above the crossing point of the two temperature branches ($\Phi_R = 0.58\Phi_0$). Logic state [1] is written by applying a magnetic flux pulse $\Phi_W = 0.87\Phi_0$, and corresponds to $T_N \simeq 886$ mK. The erasing operation is implemented by a counter pulse $\Phi_E = 0.29\Phi_0$, and results in $T_N \simeq 881$ mK (i.e., logic state [0]). Notably, the T-SQUIPT writing/erasing operations were performed several times with high reproducibility.

Stability with respect to magnetic flux fluctuations is one of the key parameters of a memory cell. Here, the stability is investigated by superimposing a sinusoidal oscillation ($\Phi_{AC} = 0.04\Phi_0$) onto the read-out flux, as shown in Fig. 4c for $P_{in} = 4.5$ pW and $\Phi_R = 0.58\Phi_0$. Despite the flux oscillations amplitude is $\sim 80\%$ of the difference between Φ_R and the minimum writing flux ($\Phi_{R,max} = 0.63\Phi_0$), the stored state is fully preserved in time. As a consequence, we can conclude that the T-SQUIPT is a thermal memory element robust against magnetic fluctuations.

Finally, a *non-volatile* memory retains the stored state when power is temporarily switched off. This property is crucial for energy saving and to design long-term persistent storage units. The operation of the T-SQUIPT as a thermal memory requires a source to generate the read-out flux Φ_R and a power generator for the thermal bias. Despite we provide Φ_R with an external superconducting coil, the read-out flux could be generated by a permanent ferromagnet without the need of an external source. Therefore, the non-volatility of the T-SQUIPT is simply investigated by turning on the heat input power only during the read-out operation, as shown in Fig. 4d.

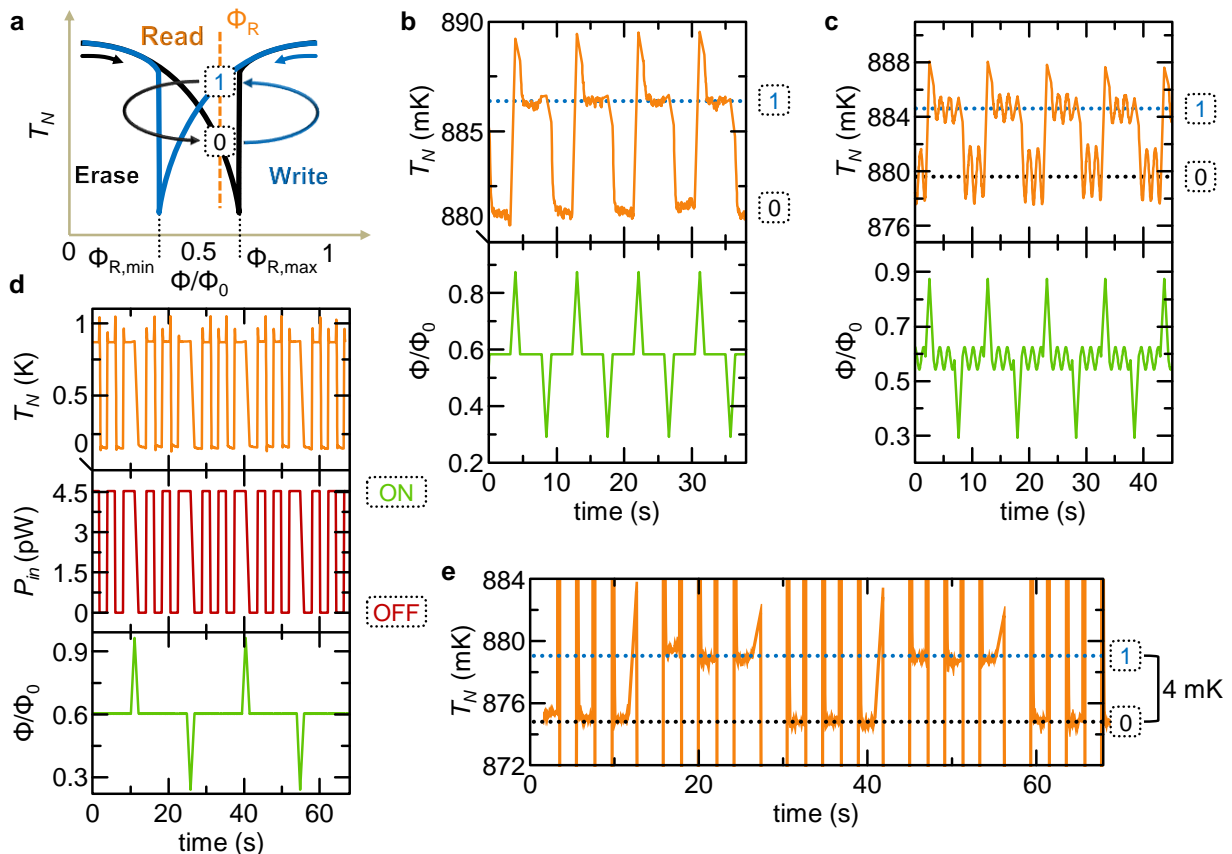


FIG. 4. **T-SQUIPT operated as thermal memory cell.** **a** Schematic representation of the T-SQUIPT operation as thermal memory cell. The logic states are encoded in low $T_{[0]}$ (black) and high $T_{[1]}$ (blue) temperature branches present at the read-out flux $\Phi_R \in (0.5\Phi_0, \Phi_{R,max})$. The write operation is performed by applying $\Phi_W > \Phi_{R,max}$, while the erase procedure consists on flux biasing the T-SQUIPT at $\Phi_E < \Phi_{R,min}$. **b** Dependence of the read-out electronic temperature T_N (top panel) on the magnetic flux (bottom panel) measured for $P_{in} = 4.5$ pW. The read-out flux is $\Phi_R = 0.58\Phi_0$, the write pulse reaches $\Phi_W = 0.87\Phi_0$ and the erase flux is $\Phi_E = 0.29\Phi_0$. **c** Dependence of the read-out electronic temperature T_N (top panel) on the magnetic flux (bottom panel) measured for $P_{in} = 4.5$ pW. The read-out flux is the sum of the constant component $\Phi = 0.58\Phi_0$ and a sinusoidal oscillation $\Phi_{AC} = \pm 0.04\Phi_0$. The write and erase fluxes are $\Phi_W = 0.87\Phi_0$ and $\Phi_E = 0.29\Phi_0$, respectively. **d** Dependence of the read-out temperature (top panel) on the magnetic flux (bottom panel). The T-SQUIPT is powered (at $P_{in} = 4.5$ pW, central panel) only during the read-out operation (at $\Phi_R = 0.58\Phi_0$). The write and erase fluxes are $\Phi_W = 0.96\Phi_0$ and $\Phi_E = 0.21\Phi_0$, respectively. **e** Zoom of the read-out electronic temperature T_N around state [0] and state [1] measured for $P_{in} = 4.5$ pW. The difference between the two memory states is ~ 4 mK.

On the one hand, for $P_{in} = 0$ the steady-state electronic temperature in N is always $T_N = T_b = 25$ mK, as expected. On the other hand, T_N can acquire two distinct values (corresponding to logic state [0] or [1]) when the T-SQUIPT is powered (see top panel of Fig. 4d and Fig. 4e). Furthermore, the stored data is not deteriorated by de-powering the memory cell. Indeed, the temperature values corresponding to state [0] ($T_{[0]} \simeq 875$ mK) and [1] ($T_{[1]} \simeq 879$ mK) remain constant in time after many powering/de-powering cycles (see Fig. 4e). Therefore, the T-SQUIPT can be, in principle, employed as a non-volatile memory cell.

In conclusion, we have demonstrated phase-tuning of the thermal properties of a nanosized superconductor by proximity effect. In particular, our thermal superconducting quantum interference proximity transistor al-

lows a fine magnetic-flux-tuning of the heat current flowing from a normal metal electrode to a tunnel-coupled proximitized superconducting nanowire. The T-SQUIPT shows electronic temperature modulations up to ~ 16 mK and flux-to-temperature transfer functions reaching ~ 60 mK/ Φ_0 around $0.5\Phi_0$. The nanovalve operates up to 1 K showing a reduction of temperature swing of $\sim 80\%$. In addition, the $T_N(\Phi)$ characteristics show also hysteresis, owing to the strong activation energy for the nucleation of a phase-slip in the proximitized nanowire. This prevents unwanted phase-slips to occur making the T-SQUIPT a prototypical thermal memory cell, where the logic state is encoded in the electronic temperature T_N . Our memory element showed robustness against magnetic flux fluctuations and non-volatility, as its electrical counterpart [17].

From the technological side, thermal control of heat currents via proximity effect might be improved by exploiting different materials configurations. For instance, the use of *short* Josephson weak-links could enhance the on/off ratio of the thermal valve [13], since the modulation of φ would be more efficient [8, 26]. Yet, the T-SQUIPT operation might be pushed above liquid helium temperature by exploiting interferometers made of larger gap superconductors, such as vanadium [27] or niobium [28]. Despite the relevance in nanoscale heat management [1, 29] and thermodynamics [30], the T-SQUIPT could find application in coherent caloritronics [11–13]. For example, it might perhaps be at the core of temperature amplifiers [14], heat logic architectures [15] or non-volatile data storage units [9, 10].

METHODS

Thermal current through a temperature-biased NIS tunnel junction

The thermal current flowing out of the N electrode of a temperature-biased normal metal/insulator/superconductor (NIS) tunnel junction reads [1]

$$P_{NIS} = \frac{1}{e^2 R_T} \int_{-\infty}^{+\infty} dE E \mathcal{N}_S(E, T_S) \times [f_0(E, T_N) - f_0(E, T_S)], \quad (1)$$

where e is the electron charge, R_T is the normal-state tunnel resistance, T_N is the temperature of the normal metal, T_S is the temperature of the superconductor, $\mathcal{N}_S(E, T_S) = |E|/\sqrt{E^2 - E_g^2(T_S)}\Theta[E^2 - E_g^2(T_S)]$ is the normalized BCS DOS of the superconductor, $E_g(T_S)$ is the superconducting pairing potential, and $f_0(E, T_i) = [1 + \exp(E/k_B T_i)]^{-1}$ is the Fermi-Dirac distribution at temperature T_i (with $i = N, S$). In the calculations, we set $T_N = 0.1T_C$ (T_C is the superconducting critical temperature corresponding to $E_{g,0} = 200 \mu\text{eV}$), $T_S = 0.01T_C$, and $R_T = 1 \text{ k}\Omega$.

T-SQUIPT fabrication

The T-SQUIPTs were fabricated by a single electron-beam lithography (EBL) step and three-angle shadow-mask metals deposition through a suspended bilayer resist mask. The evaporation and oxidation processes were performed in an ultra-high vacuum (UHV) electron-beam evaporator (base pressure of 10^{-11} Torr). The use of the same material for the deposition of the nanowire and the ring allows to obtain a transparent interface between them. Furthermore, the room temperature exposure of

aluminum films to O_2 produces high quality tunnel junctions. Therefore, the proximitized nanowire, thermometer/heater leads, and the ring of the T-SQUIPTs were all made of Al. At first, 15 nm of $\text{Al}_{0.98}\text{Mn}_{0.02}$ was deposited at an angle of -18° to realize the N electrode. Subsequently, the sample was exposed to 60 mTorr of O_2 for 5 min in order to realize the AlO_x thin layer forming the tunnel barriers. Then, a 20-nm-thick Al layer was deposited at a tilt angle of 10° to form the superconducting nanowire and tunnel leads. As final step, 70 nm of Al was deposited at 0° to realize the superconducting ring (circumference $\sim 7.6 \mu\text{m}$, and average width $w_{R,ave} \simeq 600 \text{ nm}$).

Measurement set-up

The magneto-electric and thermal measurements of the T-SQUIPTs were performed in a ^3He - ^4He dilution refrigerator (Triton 200, Oxford Instruments) equipped with RC-filters ($R = \sim 2\text{k}\Omega$) in a temperature range from 25 mK to 1 K. The magnetic field piercing the ring was applied by a superconducting magnet driven by a low-noise current source (Series 2600, Keithley Instruments). The preliminary electric characterization was performed in a two-wire voltage-bias configuration by means of a low-noise DC voltage source (GS200, Yokogawa) and a room-temperature current preamplifier (Model 1211, DL Instruments). The SINIS thermometers [1] were biased with a current of 150 pA through a battery-powered floating source, while the heaters were piloted upon voltage biasing varied from 900 μV to 2.1 mV (GS200, Yokogawa), corresponding to about 2.2–11.8 pW injected power range. The SINIS thermometers were preliminary calibrated against a RuO_2 thermometer anchored to the mixing chamber plate of the fridge while changing the bath temperature. The voltage drop across the junctions was measured with a standard room-temperature low-noise differential preamplifier (Model 1201, DL Instruments).

T-SQUIPT parameters

The zero-temperature coherence length of the superconducting proximitized wire is $\xi_{S',0} = \sqrt{\hbar D/E_{g',0}} \simeq 80 \text{ nm}$, where \hbar is the reduced Planck constant, $D = 22.5 \text{ cm}^2\text{s}^{-1}$ is the diffusion coefficient of the aluminum film, and $E_{g',0} \simeq 200 \mu\text{eV}$ is the Al zero-temperature energy gap. The S' critical temperature is $T_{C,S'} = E_{g',0}/1.764k_B \simeq 1.31 \text{ K}$, where k_B is the Boltzmann constant.

At low temperature, the ratio $L/\xi_{S',0} \simeq 4.6$, where $L = 380 \text{ nm}$ is the nanowire physical length. As a consequence, the T-SQUIPT operates in the long junction limit [3]. Non hysteretic behavior of the T-SQUIPT is expected for $\xi_{S',\text{short}} \gtrsim L/3.5 \sim 105 \text{ nm}$ [3] providing a temperature upper boundary $T_{\text{single}} =$

$T_{C,S'}(1 - 0.852^2 \xi_{S',0l}/\xi_{S',\text{short}}^2) \sim 1.29$ K [3, 16], where $l = 3D/v_F \simeq 3.3$ nm is the aluminum film mean free path, and $v_F = 2.03 \times 10^6$ m/s is the Fermi velocity of Al.

Thermal exchange in the normal metal reservoir

The energy balance equation describing the thermal steady state of the N island in the T-SQUIPT reads [1, 11]

$$P_{in} = P_{e-ph,N} + P_{th} + P_{NIS'}(\Phi). \quad (2)$$

In the above equation, $P_{e-ph,N} = \Sigma_N \mathcal{V}_N (T_N^6 - T_b^6)$ is the heat current flowing between electrons and phonons in N [1], with $\Sigma_N = 4 \times 10^9$ WK⁻⁶m⁻³ the electron-phonon coupling constant of Al_{0.98}Mn_{0.02}. P_{th} is the total thermal current flowing between N and the thermometers. The contribution of each thermometer is given by Eq. 1, where $T_S = T_b$ and the voltage drop V is present only for the energized junctions. Finally, the tunnel current flowing from N to the proximitized nanowire ($P_{NIS'}$) can be computed from Eq. 1, where the density of states of S' ($\mathcal{N}_{S'}$) takes different form depending on the sweep direction of the magnetic flux [8]. As a consequence, $P_{NIS'}$ turns out to be hysteretic with the direction of Φ .

DATA AVAILABILITY

All other data that support the plots within this paper and other findings of this study are available from the corresponding author upon reasonable request.

ACKNOWLEDGEMENTS

We acknowledge the European Research Council under Grant Agreement No. 899315-TERASEC, and the EU's Horizon 2020 research and innovation program under Grant Agreement No. 800923 (SUPERTED) and No. 964398 (SUPERGATE) for partial financial support.

AUTHOR CONTRIBUTIONS

E.S. and F.G. conceived the experiment. N.L. fabricated the samples with inputs of F.P.. N.L., F.P. and E.S. performed the measurements. N.L. analysed the experimental data with inputs from F.P., E.S., and F.G.. N.L and F.P. wrote the manuscript with inputs from all authors. All authors discussed the results and their implications equally at all stages.

ADDITIONAL INFORMATION

The authors declare no competing interests.

-
- [1] Giazotto, F., Heikkilä, T. T., Luukanen, A., Savin, A. M., & Pekola J. P. Opportunities for mesoscopies in thermometry and refrigeration: Physics and applications. *Rev. Mod. Phys.* **78**, 217-274 (2006).
- [2] de Gennes *Superconductivity of Metals and Alloys* (W. A. Benjamin, New York, 1966).
- [3] Likharev, K. K. Superconducting weak links. *Rev. Mod. Phys.* **51**, 100-159 (1979).
- [4] Eom, J., Chien, C.-J., & Chandrasekhar, V. Phase Dependent Thermopower in Andreev Interferometers. *Phys. Rev. Lett.* **81**, 437-440 (1998).
- [5] Jiang, Z., & Chandrasekhar, V. Quantitative measurements of the thermal resistance of Andreev interferometers. *Phys. Rev. B* **72**, 020502(R) (2005).
- [6] Parsons, A., Sosnin, I. A., & Petrashov, V. T. Reversal of thermopower oscillations in the mesoscopic Andreev interferometer. *Phys. Rev. B* **67**, 140502(R) (2003).
- [7] Giazotto, F., Peltonen, J., Meschke, M. et al. Superconducting quantum interference proximity transistor. *Nature Phys.* **6**, 254-259 (2010).
- [8] Virtanen, P., Ronzani, A., & Giazotto, F. Spectral Characteristics of a Fully Superconducting SQUIPT. *Phys. Rev. Appl.* **6**, 054002 (2016).
- [9] Fornieri, A., Timossi, G., Bosisio, R., Solinas, P. & Giazotto, F. Negative differential thermal conductance and heat amplification in superconducting hybrid devices. *Phys. Rev. B* **93**, 134508 (2016).
- [10] Guarcello, C., Solinas, P., Braggio, A., Di Ventra, M., & Giazotto, F. Josephson Thermal Memory. *Phys. Rev. Appl.* **9**, 014021 (2018).
- [11] Fornieri, A., & Giazotto, F. Towards phase-coherent caloritronics in superconducting circuits. *Nat. Nanotech.* **12**, 944-952 (2017).
- [12] Hwang, S.-Y., & Sothmann, B. Phase-coherent caloritronics with ordinary and topological Josephson junctions. *Eur. Phys. J. Special Topics* **229**, 683-705 (2020).
- [13] Strambini, E., Bergeret, F. S., & Giazotto, F. Proximity nanovalve with large phase-tunable thermal conductance. *Appl. Phys. Lett.* **105**, 082601 (2014).
- [14] Paolucci, F., Marchegiani, G., Strambini, E., & Giazotto, F. Phase-tunable temperature amplifier. *EPL* **118**, 68004 (2017).
- [15] Paolucci, F., Marchegiani, G., Strambini, E., & Giazotto, F. Phase-Tunable Thermal Logic: Computation with Heat. *Phys. Rev. Appl.* **10**, 024003 (2018).
- [16] Tinkham, M. *Introduction to Superconductivity* (McGraw-Hill,1996).
- [17] Ligato, N., Strambini, E., Paolucci, F., & Giazotto, F. Josephson Phase-Slip Memory with Topological Protection. *arXiv:2005.14298*, to be published in *Nat. Commun.* (2021).

- [18] Little, W. A. Decay of Persistent Currents in Small Superconductors. *Phys. Rev.* **156**, 396-403 (1967).
- [19] Giazotto, F., & Martínez-Pérez, M. The Josephson heat interferometer. *Nature* **492**, 401-405 (2012).
- [20] Fornieri, A., Timossi, G., Virtanen, P., Solinas, P., & Giazotto, F. $0-\pi$ phase-controllable thermal Josephson junction. *Nat. Nanotech* **12**, 425-429 (2017).
- [21] Wellstood, F. C., Urbina, C., & Clarke, J. Hot-electron effects in metals. *Phys. Rev. B* **49**, 5942-5955 (1994).
- [22] Baek, B., Rippard, W. H., Ben, S. P., Russek, S. E., & Dresselhaus, P. D. Hybrid superconducting-magnetic memory device using competing order parameters. *Nat. Commun.* **5**, 3888 (2014).
- [23] Golod, T., Iovan, A., & Krasnov, V.M. Single Abrikosov vortices as quantized information bits. *Nat. Commun.* **6**, 8628 (2015).
- [24] Gingrich, E.C., Niedzielski, B N., Glick, J. A., Wang, Y., Miller, D. L., Loloee, R., Pratt Jr, W. P., & Birge, N. O. Controllable $0-\pi$ Josephson junctions containing a ferromagnetic spin valve. *Nature Phys.* **12**, 564-567 (2016).
- [25] Petkovic, I., Lollo, A., Glazman, L. I., & Har, J. G. E. Deterministic phase slips in mesoscopic superconducting rings. *Nat. Commun.* **7**, 1-7 (2016).
- [26] Ronzani, A., Altimiras, C., & Giazotto, F. Highly Sensitive Superconducting Quantum-Interference Proximity Transistor. *Phys. Rev. Appl.* **2**, 024005 (2014).
- [27] Ligato, N., Marchegiani, G., Virtanen, P., Strambini, E., & Giazotto, F. High operating temperature in V-based superconducting quantum interference proximity transistors. *Sci. Rep.* **7**, 8810 (2017).
- [28] Jabdaraghi, R. N., Peltonen, J. T., Saira, O. P., & Pekola, J. P. Low-temperature characterization of Nb-Cu-Nb weak links with Ar ion-cleaned interfaces. *Appl. Phys. Lett.* **108**, 042604 (2016).
- [29] Pop, E. Energy dissipation and transport in nanoscale devices. *Nano Res.* **3**, 147-169 (2010).
- [30] Benenti, G., Casati, G., Saito, K., & Whitney, R. Fundamental aspects of steady-state conversion of heat to work at the nanoscale. *Phys. Rep.* **694**, 1 (2017).